

Charge fluctuations from molecular simulations in the constant-potential ensemble

Laura Scalfi, David T. Limmer, Alessandro Coretti, Sara Bonella, Paul A. Madden, Mathieu Salanne, Benjamin Rotenberg

▶ **To cite this version:**

Laura Scalfi, David T. Limmer, Alessandro Coretti, Sara Bonella, Paul A. Madden, et al.. Charge fluctuations from molecular simulations in the constant-potential ensemble. Physical Chemistry Chemical Physics, 2020, 22 (19), pp.10480-10489. 10.1039/C9CP06285H . hal-02869879

HAL Id: hal-02869879

https://hal.sorbonne-universite.fr/hal-02869879

Submitted on 16 Jun 2020

HAL is a multi-disciplinary open access archive for the deposit and dissemination of scientific research documents, whether they are published or not. The documents may come from teaching and research institutions in France or abroad, or from public or private research centers.

L'archive ouverte pluridisciplinaire **HAL**, est destinée au dépôt et à la diffusion de documents scientifiques de niveau recherche, publiés ou non, émanant des établissements d'enseignement et de recherche français ou étrangers, des laboratoires publics ou privés.

Charge fluctuations from molecular simulations in the constant-potential ensemble

Laura Scalfi,[a] David Limmer,[b,c,d,e] Alessandro Coretti,[f,g] Sara Bonella,[g]
Paul A. Madden,[h] Mathieu Salanne,[a,i] and Benjamin Rotenberg*[a,i]

[a] *Sorbonne Université, CNRS, Physicochimie des Électrolytes et Nanosystèmes Interfaciaux, F-75005 Paris, France.*
[b] *Department of Chemistry, University of California, Berkeley, CA, USA.*
[c] *Kavli Energy NanoScience Institute, Berkeley, CA, USA.*
[d] *Materials Science Division, Lawrence Berkeley National Lab., Berkeley, CA, USA.*
[e] *Chemical Science Division, Lawrence Berkeley National Lab., Berkeley, CA, USA.*
[f] *Department of Mathematical Sciences, Politecnico di Torino, I-10129 Torino, Italy.*
[g] *Centre Européen de Calcul Atomique et Moléculaire (CECAM), Ecole Polytechnique Fédérale de Lausanne, 1015 Lausanne, Switzerland.*
[h] *Department of Materials, University of Oxford, Oxford, UK.*
[i] *Réseau sur le Stockage Electrochimique de l'Energie (RS2E), FR CNRS 3459, France.*
* *Tel/Fax: +33144272203/3228; E-mail: benjamin.rotenberg@sorbonne-universite.fr*

We revisit the statistical mechanics of charge fluctuations in capacitors. In constant-potential classical molecular simulations, the atomic charge of electrode atoms are treated as additional degrees of freedom which evolve in time so as to satisfy the constraint of fixed electrostatic potential for each configuration of the electrolyte. The present work clarifies the role of the overall electroneutrality constraint, as well as the link between the averages computed within the Born-Oppenheimer approximation and that of the full constant-potential ensemble. This allows us in particular to derive a complete fluctuation-dissipation relation for the differential capacitance, that includes a contribution from the charge fluctuations (around the charges satisfying the constant-potential and electroneutrality constraints) also present in the absence of an electrolyte. We provide a simple expression for this contribution from the elements of the inverse of the matrix defining the quadratic form of the fluctuating charges in the energy. We then illustrate numerically the validity of our results, and recover the expected continuum result for an empty capacitor with structureless electrodes at large inter-electrode distances. By considering a variety of liquids between graphite electrodes, we confirm that this contribution to the total differential capacitance is small compared to that induced by the thermal fluctuations of the electrolyte.

PACS numbers:

I. INTRODUCTION

The electrode-electrolyte interface, where a metallic solid meets an ionic fluid, is at the heart of all electrochemistry and of many applications including sensors [1], energy storage in batteries [2] and supercapacitors [3], or the harvesting of energy from sunlight [4] or salinity gradients in estuaries [5]. In order to go beyond the traditional picture of electric double layers in electrolytes or its extensions for ionic liquids (see *e.g.* Refs. 6, 7 for reviews), molecular simulation has become an essential tool to investigate the properties of such interfaces, providing both new fundamental understanding [8, 9] and insights for practical applications [10–14].

A description of the electronic structure of the metal requires in principle *ab initio* calculations, usually at the Density Functional Theory level, but their computational cost limits the size of the simulated system on the liquid side, or introduces drastic simplification of its description, *e.g.* using an implicit polarizable model. As a result, classical molecular dynamics has become the standard approach to describe the interfacial liquid and sample its configurations over the relevant length and time scales. This requires in turn an appropriate description of the metal. While treating the electrodes as uniformly charged, structureless or atomically resolved walls has been common practice, several studies underlined the importance of accounting for the polarization of the metal by the interfacial ions and molecules [15–19]. In specific geometries, the continuum picture of image charges can be exploited to compute the electrostatic interactions in simulations of explicit electrolytes between implicit walls [17, 20].

A more flexible approach, allowing the atomic structure of the electrode to be captured as well, is to treat the charge of each electrode atom as an additional degree of freedom, which fluctuates in response to the microscopic configuration of the electrolyte in order to maintain the electrode at a constant potential rather than charge. This approach, described in more detail below, was proposed by Siepmann and Sprik to model the tip of a scanning tunneling microscope approaching a planar metal surface[21], and later adapted by Reed *et al.* to the case of an electrochemical cell[22]. The use of (Gaussian) charge distributions with fluctuating magnitude to represent the electrode atoms opened the way to the simulation of a variety of electrochemical systems, involving platinum and carbon electrodes and a variety of liquids including molten salts, pure water, aqueous or organic solutions of electrolytes, room temperature ionic liquids and water-in-salts [23–29]. Since then, other approaches have been proposed to account

for the polarization of the metal in response to its environment, which share with the Siepmann and Sprik model the treatment of the atomic charges as additional degrees of freedom and the expression of the energy of the system as a quadratic form of these charges, but differ in the coefficients of this form. It was derived from a tight-binding approximation in Ref. 30 and from electronegativity equalization considerations in Ref. 31.

An important consequence of imposing the potential of the electrodes is that their charge fluctuates. Such charge fluctuations in electrical circuits have been identified as a source of information on the system by Nyquist and Johnson[32, 33], who derived a relation between the differential capacitance and the variance of the charge fluctuations. Charge fluctuations are also exploited to infer information on redox reactions and corrosion processes [34, 35] or more recently for sensing in nanofluidic channels [36–38]. On the theoretical side, the charge fluctuations in constant-potential simulations have been investigated using *ab initio* simulations [39] as well as with the primitive model of electrolytes between (fluctuating) uniformly charged smooth electrodes [40].

In previous work [41], the charge fluctuations in molecular dynamics simulations of nanocapacitors described by the fluctuating charge model of electrodes was examined. In particular, it was shown how histogram reweighting techniques can be used to sample the properties of nanocapacitors as a function of voltage and to efficiently evaluate the differential capacitance in such simulations. This allowed a voltage-induced order-disorder transition to be identified in the first adsorbed layer of a room temperature ionic liquid on graphite, associated with a peak in differential capacitance [42, 43], and to study the effects of solution composition on the electrochemical response of a double layer capacitor [44]. Haskins and Lawson later identified an additional contribution to the capacitance of the system, representing "the self-capacitance of the electrodes under the influence of the electrolyte structure", which they found to be small (though non-negligible) and relatively insensitive to the value of voltage for the considered systems [18].

In the present work, we revisit the statistical mechanics of the constant-potential ensemble, for the generic case where the energy is a quadratic form of the fluctuating charges. To enable a closed description of the system, *i.e.* one that does not require to take explicitly into account interactions with a charge reservoir such as a generator, we introduce explicitly the constraint of global electroneutrality of the system. This constraint, consistent with previous works, also ensures that relevant physical properties such as the capacitance depend only on the potential difference between the electrodes and not on the absolute potentials. Within this model, we investigate the sampling of the constant-potential ensemble in molecular simulations. While in principle the full phase space corresponds to treating electrolyte configurations and electrode charges on equal terms as degrees of freedom, in practice most simulations are performed within the Born-Oppenheimer approximation, where a single set of electrode charges corresponds to each electrolyte configuration. By comparing the two associated probability distributions, we discuss the possibility of computing observables via Born-Oppenheimer sampling.

We obtain explicit analytical results for a number of properties, including the configuration-dependent potential shift previously introduced as a Lagrange multiplier to enforce the electroneutrality constraint, the configuration-dependent set of charges satisfying the constant-potential and electroneutrality constraints and the differential capacitance of the system. We obtain an explicit expression for the term identified as the self-capacitance in Ref. 18, which we show to be independent not only of voltage but also of the configuration of the electrolyte. This term, which corresponds to the capacitance of the electrolyte-free capacitor, is expressed simply from the elements of the inverse of the matrix defining the quadratic form of the fluctuating charges in the energy. We then illustrate numerically the validity of our results, and recover in particular, at large inter-electrode distance, the expected result for an empty capacitor with structureless electrodes. By considering pure water, an aqueous electrolyte solution and a room temperature ionic liquid between graphite electrodes, we confirm that this contribution to the total differential capacitance is small compared to that induced by the thermal fluctuations of the electrolyte. Theoretical results are introduced and derived in Section II, while applications are considered in Section III.

II. STATISTICAL MECHANICS OF THE CONSTANT-POTENTIAL ENSEMBLE

The classical description of metallic electrodes with fluctuating charges[21, 22] involves mobile ions and molecules of the electrolyte, with N atomic positions $\mathbf{r}^N$ and momenta $\mathbf{p}^N$, as well as M immobile electrode atoms with atom-centered charge distributions (such as point charges or Gaussians) with fluctuating magnitudes $\mathbf{q} = \{q_1, \dots, q_M\}$. While the following derivations can be extended to the case of mobile electrode atoms (or at least mobile rigid electrodes) by introducing the corresponding degrees of freedom, we will restrict ourselves to the case of fixed electrodes for simplicity. The Hamiltonian of the system is written as

$$\mathcal{H}(\mathbf{r}^N, \mathbf{p}^N, \mathbf{q}) = \mathcal{K}(\mathbf{p}^N) + \mathcal{U}_0(\mathbf{r}^N) + \mathcal{U}_{el}(\mathbf{r}^N, \mathbf{q}) \,, \tag{1}$$

with $\mathcal{K}$ the kinetic energy of the electrolyte, and where the potential energy is split into $\mathcal{U}_{el}(\mathbf{r}^N, \mathbf{q})$, the electrostatic interaction involving the fluctuating charges (both between them and with the electrolyte), and $\mathcal{U}_0(\mathbf{r}^N)$, which contains all other terms: electrostatic interactions within the electrolyte and all the non-electrostatic terms within the

electrolyte and with the electrode atoms. The electrostatic term involving the fluctuating charges is quadratic in the charges, written as

$$\mathcal{U}_{el}(\mathbf{r}^N, \mathbf{q}) = \frac{\mathbf{q}^T \mathbf{A} \mathbf{q}}{2} - \mathbf{q}^T \mathbf{B}(\mathbf{r}^N) \, , \tag{2}$$

where the symmetric $M \times M$ matrix $\mathbf{A}$ depends on the positions of the electrode atoms and the parameters describing the charge distribution on each atom, while the components of the vector $\mathbf{B}(\mathbf{r}^N)$ are the electrostatic potential due to the electrolyte on each electrode atom. Explicit expressions for $\mathbf{A}$ and $\mathbf{B}(\mathbf{r}^N)$ for the particular case of Gaussian charge distributions, taking into account two-dimensional Ewald summation for electrostatic interactions, can be found in Refs. 22, 45. The set of electrostatic potentials on each electrode atom is given by the gradient of $\mathcal{U}_{el}$ with respect to $\mathbf{q}^T$,

$$\frac{\partial \mathcal{U}_{el}(\mathbf{r}^N, \mathbf{q})}{\partial \mathbf{q}^T} = \mathbf{A}\mathbf{q} - \mathbf{B}(\mathbf{r}^N) \, , \tag{3}$$

and depends on the positions of the electrode atoms and on the electrolyte configuration.

A. Constant-potential ensemble

We consider the constant-potential ensemble in which the electrostatic potential on each electrode atom is fixed to a prescribed value. In addition, the number N of electrolyte atoms, the number M of electrode atoms, the volume V of the system and the temperature T are also considered as fixed in the present work. We consider a capacitor with two electrodes with potentials ψ_L and ψ_R and corresponding voltage,

$$\Delta\psi = \psi_L - \psi_R \, , \tag{4}$$

with electrode atoms ordered such that the first M_L correspond to the left electrode and the remaining M_R to the right electrode. We form the vector of constant potentials

$$\Psi^T = (\underbrace{\psi_L, \ldots, \psi_L}_{M_L \text{ atoms}}, \underbrace{\psi_R, \ldots, \psi_R}_{M_R \text{ atoms}}) = \Delta\psi \mathbf{D}^T + \bar{\psi}\mathbf{E}^T \, , \tag{5}$$

where we have introduced the average potential

$$\bar{\psi} = \frac{M_L\psi_L + M_R\psi_R}{M_L + M_R} \tag{6}$$

and two constant, orthogonal vectors

$$\mathbf{E}^T = (1, \ldots, 1) \quad \text{and} \quad \mathbf{D}^T = (\underbrace{\alpha_L, \ldots, \alpha_L}_{M_L \text{ atoms}}, \underbrace{\alpha_R, \ldots, \alpha_R}_{M_R \text{ atoms}}) \, , \tag{7}$$

with

$$\alpha_L = \frac{M_R}{M_L + M_R} \quad \text{and} \quad \alpha_R = \alpha_L - 1 = -\frac{M_L}{M_L + M_R} \, . \tag{8}$$

For symmetric capacitors, $M_L = M_R$ and the components of $\mathbf{D}$ are equal to $\pm\frac{1}{2}$. The total charge on both electrodes is given by

$$Q_{tot} = Q_L + Q_R = \sum_{i=1}^{M_L} q_i + \sum_{i=M_L+1}^{M_L+M_R} q_i = \mathbf{q}^T \mathbf{E} \, . \tag{9}$$

With this notation, the constraint of global charge electroneutrality (to be discussed in the next section) can be compactly written as

$$\mathbf{q}^T \mathbf{E} = \mathbf{E}^T \mathbf{q} = 0 \, . \tag{10}$$

Then the total charges of the two electrodes are equal in magnitude and of opposite sign, which is conveniently expressed as

$$Q_L = -Q_R = \mathbf{q}^T\mathbf{D} = \mathbf{D}^T\mathbf{q} \ . \tag{11}$$

Similarly, from Eq. 10, the product between charges and potentials simplifies to

$$\mathbf{\Psi}^T\mathbf{q} = \mathbf{q}^T\mathbf{\Psi} = \Delta\psi\mathbf{D}^T\mathbf{q} = Q_L\Delta\psi = -Q_R\Delta\psi \ . \tag{12}$$

This quantity corresponds to the work exchanged with a charge reservoir (the external circuit which connects the two electrodes) when charging the capacitor from $\mathbf{q} = 0$ to a charge distribution $\mathbf{q}$ under the fixed potentials $\mathbf{\Psi}$.

B. Partition function

In the constant-potential ensemble, the charge distribution $\mathbf{q}$ on the electrodes fluctuates and the corresponding partition function is an integral over electrolyte configurations (we do not consider the fluctuations of the conjugate momenta of the electrolyte, which are statistically independent) and electrode charge distributions. Two important points must be taken into account to compute this partition function. The Boltzmann factor needs to include the work $\mathbf{q}^T\mathbf{\Psi}$ in addition to the Hamiltonian Eq. 1, which arises from the Legendre transform between constant-charge and constant-potential ensembles. Additionally, we enforce the constraint of global electroneutrality, Eq. 10, considering that charge is transferred from one electrode to the other, keeping the total charge of the system unchanged. The partition function therefore reads

$$\begin{aligned}\mathcal{Z} &= \int \mathrm{d}\mathbf{r}^N \int \mathrm{d}\mathbf{q}\ e^{-\beta\left[\mathcal{U}_0(\mathbf{r}^N)+\frac{\mathbf{q}^T\mathbf{A}\mathbf{q}}{2}-\mathbf{q}^T\mathbf{B}(\mathbf{r}^N)-\mathbf{q}^T\mathbf{\Psi}\right]}\delta(\beta\mathbf{q}^T\mathbf{E}) \\ &= \int \mathrm{d}\mathbf{r}^N\ e^{-\beta\mathcal{U}_0(\mathbf{r}^N)} \int \mathrm{d}\mathbf{q}\ e^{-\beta\left[\frac{\mathbf{q}^T\mathbf{A}\mathbf{q}}{2}-\mathbf{q}^T(\mathbf{B}(\mathbf{r}^N)+\mathbf{\Psi})\right]}\delta(\beta\mathbf{q}^T\mathbf{E}) \ ,\end{aligned} \tag{13}$$

where $\beta = 1/k_BT$, with k_B Boltzmann's constant, and the Dirac δ function ensures that only charge distributions satisfying global neutrality are considered.

In order to perform the constrained Gaussian integral over the charge distributions in Eq. 13, we introduce the Fourier representation of the Dirac function as

$$\delta(\beta\mathbf{q}^T\mathbf{E}) = \frac{1}{2\pi}\int_{-\infty}^{+\infty}\mathrm{d}k\ e^{ik\beta\mathbf{q}^T\mathbf{E}} \ . \tag{14}$$

We then reverse the order of the integrations over $\mathbf{q}$ and k and perform first the Gaussian integral over $\mathbf{q}$:

$$\begin{aligned}\mathcal{Z} &= \int \mathrm{d}\mathbf{r}^N\ e^{-\beta\mathcal{U}_0(\mathbf{r}^N)}\frac{1}{2\pi}\int_{-\infty}^{+\infty}\mathrm{d}k\int \mathrm{d}\mathbf{q}\ e^{-\beta\left[\frac{\mathbf{q}^T\mathbf{A}\mathbf{q}}{2}-\mathbf{q}^T(\mathbf{B}(\mathbf{r}^N)+\mathbf{\Psi}+ik\mathbf{E})\right]} \\ &= \frac{1}{2\pi}\sqrt{\frac{(2\pi)^M}{\beta^M\det\mathbf{A}}}\int \mathrm{d}\mathbf{r}^N\ e^{-\beta\mathcal{U}_0(\mathbf{r}^N)}\times \\ &\qquad e^{+\frac{\beta}{2}\left[\mathbf{B}(\mathbf{r}^N)+\mathbf{\Psi}\right]^T\mathbf{A}^{-1}\left[\mathbf{B}(\mathbf{r}^N)+\mathbf{\Psi}\right]}\int_{-\infty}^{+\infty}\mathrm{d}k\ e^{-\alpha k^2+\gamma k}\end{aligned} \tag{15}$$

where we have introduced the scalars $\alpha = \frac{\beta}{2}\mathbf{E}^T\mathbf{A}^{-1}\mathbf{E}$ and $\gamma = i\beta\mathbf{E}^T\mathbf{A}^{-1}\left[\mathbf{B}(\mathbf{r}^N)+\mathbf{\Psi}\right]$. Performing the Gaussian integral over k and after some simple algebra, we can rewrite

$$\mathcal{Z} = K\int \mathrm{d}\mathbf{r}^N\ e^{-\beta\mathcal{U}_0(\mathbf{r}^N)}e^{+\frac{\beta}{2}\left[\mathbf{B}(\mathbf{r}^N)+\mathbf{\Psi}-\chi(\mathbf{r}^N)\mathbf{E}\right]^T\mathbf{A}^{-1}\left[\mathbf{B}(\mathbf{r}^N)+\mathbf{\Psi}-\chi(\mathbf{r}^N)\mathbf{E}\right]} \tag{16}$$

with a prefactor

$$K = \frac{1}{2\pi}\sqrt{\frac{(2\pi)^M}{\beta^M\det\mathbf{A}}}\sqrt{\frac{2\pi}{\beta\mathbf{E}^T\mathbf{A}^{-1}\mathbf{E}}} \ , \tag{17}$$

and where we introduced the scalar

$$\chi(\mathbf{r}^N) = \frac{1}{\mathbf{E}^T\mathbf{A}^{-1}\mathbf{E}}\mathbf{E}^T\mathbf{A}^{-1}\left[\mathbf{B}(\mathbf{r}^N) + \mathbf{\Psi}\right] \ . \tag{18}$$

This quantity can be interpreted as a configuration-dependent potential shift, since $\mathbf{\Psi} - \chi\mathbf{E}$ simply changes all values of the potentials by a constant. This additional constant is a Lagrange multiplier enforcing the electroneutrality constraint, but leaving the voltage between the electrodes invariant. The present derivation provides an explicit expression of this configuration-dependent potential shift $\chi(\mathbf{r}^N)$ enforcing electroneutrality.

C. Sampling the constant-potential ensemble with Born-Oppenheimer dynamics

In classical simulations, the constant-potential ensemble can be sampled using either Monte Carlo simulations or molecular dynamics. Siepmann and Sprik first proposed in Ref. 21 to use Car-Parrinello dynamics by introducing fictitious dynamics for the charge degrees of freedom. Reed *et al.* later used Born-Oppenheimer dynamics in Ref. 22, in which the additional degrees of freedom $\mathbf{q}$ are relaxed at each timestep by imposing the constraint of constant-potential on the charges

$$\frac{\partial \mathcal{U}_{el}(\mathbf{r}^N, \mathbf{q})}{\partial \mathbf{q}^T} = \Psi \ . \tag{19}$$

Such a Born-Oppenheimer approximation is frequently used in *ab initio* molecular dynamics, which considers the electronic degrees of freedom to instantaneously adapt to the nuclei movement and thus decouples electronic and atomic degrees of freedom.

Without enforcing the electroneutrality constraint (Eq. 10), the set of charges that satisfies this constant-potential constraint is given by $\mathbf{A}^{-1}(\mathbf{B}(\mathbf{r}^N) + \Psi)$, as can be immediately seen from Eqs 3 and 19. In Eq. 16, we recognize the set of charges $\mathbf{q}^*$ satisfying both the constraints of fixed potentials and of global electroneutrality for a given configuration which is given by

$$\mathbf{q}^*(\mathbf{r}^N) = \mathbf{A}^{-1}\left[\mathbf{B}(\mathbf{r}^N) + \mathbf{\Psi} - \chi(\mathbf{r}^N)\mathbf{E}\right] = \mathbf{S}\left[\mathbf{B}(\mathbf{r}^N) + \mathbf{\Psi}\right] \ , \tag{20}$$

where we have used Eq. 18 and defined the symmetric matrix

$$\mathbf{S} \equiv \mathbf{A}^{-1} - \frac{\mathbf{A}^{-1}\mathbf{E}\mathbf{E}^T\mathbf{A}^{-1}}{\mathbf{E}^T\mathbf{A}^{-1}\mathbf{E}} \ . \tag{21}$$

We have therefore obtained an explicit expression for the configuration-dependent set of charges satisfying the constraints of fixed potentials and global electroneutrality. Note that the reference used to define the set of fixed potentials $\mathbf{\Psi}$ is irrelevant, as expected. Indeed, shifting all potentials by a constant value leads via Eq. 20 to the same set of charges.

From Eq. 16, the partition function is expressed using this particular set of charges as

$$\mathcal{Z} = K\int \mathrm{d}\mathbf{r}^N \ e^{-\beta\mathcal{U}_0(\mathbf{r}^N) + \frac{\beta}{2}[\mathbf{q}^*(\mathbf{r}^N)]^T\mathbf{A}\mathbf{q}^*(\mathbf{r}^N)} \ , \tag{22}$$

where we have introduced an equivalent expression of the electrostatic energy in the Boltzmann factor.

As highlighted earlier, the Born-Oppenheimer dynamics simulations do not sample the constant-potential ensemble. Neglecting the fluctuations of the charges around their optimum yields a partition function, $\mathcal{Z}^{\mathrm{BO}}$, which does not include the integral over the additional degrees of freedom $\mathbf{q}$, since these are now functions of the positions $\mathbf{r}^N$ and replaced by $\mathbf{q}^*(\mathbf{r}^N)$. We will write $\mathbf{q}^*$ in the following but one should bear in mind this explicit dependence on $\mathbf{r}^N$. To write $\mathcal{Z}^{\mathrm{BO}}$, we replace in Eq. 13 the integral over $\mathbf{q}$ by enforcing the constraint $\mathbf{q} = \mathbf{q}^*$ for each electrolyte configuration. Using the definition of $\mathbf{q}^*$, Eq. 20, and noting that $(\mathbf{q}^*)^T\mathbf{E} = 0$, we simplify the Boltzmann factor as

$$\mathcal{Z}^{\mathrm{BO}} = \int \mathrm{d}\mathbf{r}^N \ \ e^{-\beta\mathcal{U}_0(\mathbf{r}^N) + \frac{\beta}{2}(\mathbf{q}^*)^T\mathbf{A}\mathbf{q}^*} \ . \tag{23}$$

We can now express the probability of finding a microscopic state in each ensemble as

$$\mathcal{P}(\mathbf{r}^N, \mathbf{q}) = \frac{e^{-\beta\left[\mathcal{U}_0(\mathbf{r}^N) + \frac{\mathbf{q}^T\mathbf{A}\mathbf{q}}{2} - \mathbf{q}^T(\mathbf{B}(\mathbf{r}^N) + \mathbf{\Psi})\right]}\delta(\beta\mathbf{q}^T\mathbf{E})}{K\int \mathrm{d}\mathbf{r}^N \ e^{-\beta\mathcal{U}_0(\mathbf{r}^N) + \frac{\beta}{2}(\mathbf{q}^*)^T\mathbf{A}\mathbf{q}^*}} \tag{24}$$

$$\mathcal{P}^{\mathrm{BO}}(\mathbf{r}^N) = \frac{e^{-\beta\mathcal{U}_0(\mathbf{r}^N) + \frac{\beta}{2}(\mathbf{q}^*)^T\mathbf{A}\mathbf{q}^*}}{\int \mathrm{d}\mathbf{r}^N \ e^{-\beta\mathcal{U}_0(\mathbf{r}^N) + \frac{\beta}{2}(\mathbf{q}^*)^T\mathbf{A}\mathbf{q}^*}} \ . \tag{25}$$

Using Eq. 20 and simple algebra, it therefore follows that the probability of a given configuration $\{\mathbf{r}^N, \mathbf{q}\}$ in the constant-potential ensemble is related to the probability of a given configuration $\{\mathbf{r}^N\}$ in the Born-Oppenheimer ensemble as

$$\mathcal{P}(\mathbf{r}^N, \mathbf{q}) = \mathcal{P}^{\mathrm{BO}}(\mathbf{r}^N) K^{-1} \delta(\beta \mathbf{q}^T \mathbf{E}) e^{-\frac{\beta}{2}(\mathbf{q}-\mathbf{q}^*)^T \mathbf{A} (\mathbf{q}-\mathbf{q}^*)} \,. \tag{26}$$

We then write the probability distribution of an observable $\mathcal{O}$ in the constant-potential ensemble as

$$\begin{aligned} p(\mathcal{O}) &= \int \mathrm{d}\mathbf{r}^N \int \mathrm{d}\mathbf{q} \mathcal{P}(\mathbf{r}^N, \mathbf{q}) \delta(\mathcal{O}(\mathbf{r}^N, \mathbf{q}) - \mathcal{O}) \\ &= \int \mathrm{d}\mathbf{r}^N \; \mathcal{P}^{\mathrm{BO}}(\mathbf{r}^N) K^{-1} \int \mathrm{d}\mathbf{q} e^{-\frac{\beta}{2}(\mathbf{q}-\mathbf{q}^*)^T \mathbf{A} (\mathbf{q}-\mathbf{q}^*)} \\ &\qquad \times \delta(\beta \mathbf{q}^T \mathbf{E}) \delta(\mathcal{O}(\mathbf{r}^N, \mathbf{q}) - \mathcal{O}) \,. \end{aligned} \tag{27}$$

For observables that depend exclusively on the positions, *i.e.* $\mathcal{O}(\mathbf{r}^N, \mathbf{q}) = \mathcal{O}(\mathbf{r}^N)$, the second Dirac δ function can be moved out of the integral over $\mathbf{q}$ and, following the same steps as in Section II B, it is straightforward to show that the probability distribution in each ensemble are equal, *i.e.* $p(\mathcal{O}) = p^{\mathrm{BO}}(\mathcal{O})$. Therefore, charge-independent observables, such as density profiles or structure factors, are correctly sampled in Born-Oppenheimer simulations.

We now turn to observables expressed as

$$\mathcal{O}(\mathbf{r}^N, \mathbf{q}) = \mathcal{O}^*(\mathbf{r}^N) + (\mathbf{q} - \mathbf{q}^*)^T \mathbf{G}^*(\mathbf{r}^N) \,, \tag{28}$$

where $\mathcal{O}^*(\mathbf{r}^N) = \mathcal{O}(\mathbf{r}^N, \mathbf{q}^*)$ and $\mathbf{G}^*(\mathbf{r}^N) = \nabla_{\mathbf{q}} \mathcal{O}|_{\mathbf{q}^*}$ are the observable and its gradient taken for $\mathbf{q} = \mathbf{q}^*$ and depend only on the positions $\mathbf{r}^N$. Such observables include all linear combinations of the charges, such as the total charge of an electrode, and can serve as an approximation for more generic observables as a Taylor expansion around $\mathbf{q}^*$. To calculate the probability distribution of $\mathcal{O}$, we start by introducing the Fourier representation of both Dirac functions in Eq. 27, the second one being

$$\delta(\mathcal{O}(\mathbf{r}^N, \mathbf{q}) - \mathcal{O}) = \frac{1}{2\pi} \int_{-\infty}^{+\infty} \mathrm{d}m \; e^{im(\mathcal{O}(\mathbf{r}^N, \mathbf{q}) - \mathcal{O})} \,. \tag{29}$$

Reversing the order of the integrals, inserting Eq. 28 and carrying out the Gaussian integrals over $\mathbf{q}$ then k and m results in a compact expression

$$p(\mathcal{O}) = \int \mathrm{d}\mathbf{r}^N \; \mathcal{P}^{\mathrm{BO}}(\mathbf{r}^N) \sqrt{\frac{\beta}{2\pi [\mathbf{G}^*(\mathbf{r}^N)]^T \mathbf{S} \mathbf{G}^*(\mathbf{r}^N)}} \; e^{-\frac{\beta}{2} \frac{[\mathcal{O}^*(\mathbf{r}^N) - \mathcal{O}]^2}{[\mathbf{G}^*(\mathbf{r}^N)]^T \mathbf{S} \mathbf{G}^*(\mathbf{r}^N)}} \,, \tag{30}$$

where we used the definition of $\mathbf{S}$ in Eq. 21. This formulation shows that the Born-Oppenheimer sampling of the observable $\mathcal{O}$ lacks a contribution due to the charge degrees of freedom that is expressed here as Gaussian fluctuations of this observable around a mean value $\mathcal{O}^*(\mathbf{r}^N)$ with a variance $\beta^{-1} [\mathbf{G}^*(\mathbf{r}^N)]^T \mathbf{S} \mathbf{G}^*(\mathbf{r}^N)$.

As an example, which will be used in the next section, we apply Eq. 30 to the total charge on the left electrode, $Q_L(\mathbf{r}^N) = \mathbf{q}^T \mathbf{D} = Q_L^*(\mathbf{r}^N) + (\mathbf{q} - \mathbf{q}^*)^T \mathbf{D}$. In this particular case, the gradient $\mathbf{G}^*(\mathbf{r}^N) = \mathbf{D}$ is independent of the electrolyte positions $\mathbf{r}^N$. The average of Q_L over the full phase space corresponding to the constant-potential is easily computed as the Gaussian integral

$$\begin{aligned} \langle Q_L \rangle_{\mathbf{r}^N, \mathbf{q}} &= \int \mathrm{d}Q_L \; p(Q_L) \; Q_L \\ &= \int \mathrm{d}\mathbf{r}^N \; \mathcal{P}^{\mathrm{BO}}(\mathbf{r}^N) \sqrt{\frac{\beta}{2\pi \mathbf{D}^T \mathbf{S} \mathbf{D}}} \int \mathrm{d}Q_L \; Q_L \; e^{-\frac{\beta}{2} \frac{(Q_L^* - Q_L)^2}{\mathbf{D}^T \mathbf{S} \mathbf{D}}} \\ &= \int \mathrm{d}\mathbf{r}^N \; \mathcal{P}^{\mathrm{BO}}(\mathbf{r}^N) Q_L^*(\mathbf{r}^N) = \langle Q_L^* \rangle_{\mathbf{r}^N}^{\mathrm{BO}} \end{aligned} \tag{31}$$

and therefore coincides with the average of Q_L^* sampled in the Born-Oppenheimer approximation. Similarly, the average of Q_L^2 is given by the second moment of the distribution, which is the sum of the squared mean and the variance,

$$\begin{aligned} \left\langle Q_L^2 \right\rangle_{\mathbf{r}^N, \mathbf{q}} &= \left\langle Q_L^{*2} \right\rangle_{\mathbf{r}^N}^{\mathrm{BO}} + \beta^{-1} \left\langle \mathbf{D}^T \mathbf{S} \mathbf{D} \right\rangle_{\mathbf{r}^N}^{\mathrm{BO}} \\ &= \left\langle Q_L^{*2} \right\rangle_{\mathbf{r}^N}^{\mathrm{BO}} + \beta^{-1} \mathbf{D}^T \mathbf{S} \mathbf{D} \,, \end{aligned} \tag{32}$$

where for the second equality we have used the fact that $\mathbf{D}^T\mathbf{S}\mathbf{D}$ does not depend on the electrolyte configuration $\mathbf{r}^N$. Therefore, this second moment does not simply coincide with the average of Q_L^{*2} sampled in the Born-Oppenheimer approximation. It contains an additional contribution from the fluctuations of the charge around $\mathbf{q}^*$ for each configuration of the electrolyte. This result applies to any observable that depends linearly on the charges and proves that Born-Oppenheimer dynamics sample correctly their average value but lacks a term in their fluctuations, that we can express as a function of the gradient of the observable with respect to the charges.

D. Charge and capacitance

We now turn to the calculation of the differential capacitance which is defined as the derivative of the average charge of the electrode $\langle Q_L \rangle_{\mathbf{r}^N,\mathbf{q}}$ with respect to voltage,

$$C_{\text{diff}} = \frac{\partial \langle Q_L \rangle_{\mathbf{r}^N,\mathbf{q}}}{\partial \Delta\psi} \,. \tag{33}$$

In order to evaluate the latter, we will use the fact that the charge and differential capacitance are the first and second order derivatives of the free energy $F = -\beta^{-1} \ln \mathcal{Z}$ with respect to voltage $\Delta\psi$. From the expression of $\mathcal{Z}$ given in Eq.13, and using Eq. 12, the first derivative of the free energy is easily computed as

$$\begin{aligned} -\frac{1}{\beta}\frac{\partial \ln \mathcal{Z}}{\partial \Delta\psi} &= -\frac{1}{\beta\mathcal{Z}} \int \mathrm{d}\mathbf{r}^N \; e^{-\beta \mathcal{U}_0(\mathbf{r}^N)} \int \mathrm{d}\mathbf{q} \; (\beta \mathbf{q}^T \mathbf{D}) \\ &\qquad \times e^{-\beta\left[\frac{\mathbf{q}^T\mathbf{A}\mathbf{q}}{2} - \mathbf{q}^T(\mathbf{B}(\mathbf{r}^N)+\mathbf{\Psi})\right]} \delta(\beta \mathbf{q}^T \mathbf{E}) \\ &= -\left\langle \mathbf{q}^T \mathbf{D} \right\rangle_{\mathbf{r}^N,\mathbf{q}} = -\left\langle Q_L \right\rangle_{\mathbf{r}^N,\mathbf{q}} \end{aligned} \tag{34}$$

where the average is taken over microscopic configurations in the constant-potential ensemble. The free energy change during the charge of the capacitor, initially at zero voltage, to finite voltage $\Delta\psi_{max}$, is therefore

$$\Delta F = -\int_0^{\Delta\psi_{max}} \langle Q_L \rangle_{\mathbf{r}^N,\mathbf{q}} \, \mathrm{d}\Delta\psi \;\; = \int_0^{\Delta\psi_{max}} \langle Q_R \rangle_{\mathbf{r}^N,\mathbf{q}} \, \mathrm{d}\Delta\psi \,, \tag{35}$$

the reversible electrical work exchanged with the charge reservoir. The differential capacitance is then obtained from the second derivative of the free energy with respect to voltage as

$$C_{\text{diff}} = \frac{\partial \langle Q_L \rangle_{\mathbf{r}^N,\mathbf{q}}}{\partial \Delta\psi} = \beta \left\langle \delta Q_L^2 \right\rangle_{\mathbf{r}^N,\mathbf{q}} \,, \tag{36}$$

with $\delta Q_L = Q_L - \langle Q_L \rangle_{\mathbf{r}^N,\mathbf{q}}$. The differential capacitance C_{diff} thus corresponds to the fluctuations of the total charge on one electrode in the constant-potential ensemble. To make the link with the observables computed with Born-Oppenheimer dynamics, we introduce Eq. 31 and 32:

$$\begin{aligned} C_{\text{diff}} &= \beta \left\langle Q_L^2 \right\rangle_{\mathbf{r}^N,\mathbf{q}} - \beta \langle Q_L \rangle^2_{\mathbf{r}^N,\mathbf{q}} \\ &= \beta \left\langle Q_L^{*2} \right\rangle^{\text{BO}}_{\mathbf{r}^N} + \mathbf{D}^T\mathbf{S}\mathbf{D} - \beta \left(\langle Q_L^* \rangle^{\text{BO}}_{\mathbf{r}^N} \right)^2 \\ &= \beta \left\langle \delta Q_L^{*2} \right\rangle^{\text{BO}}_{\mathbf{r}^N} + \mathbf{D}^T\mathbf{S}\mathbf{D} \,. \end{aligned} \tag{37}$$

This is the main practical result of the present work. Compared to the result of Ref. 41, where the last term was missing, and to Ref. 18, the present derivation shows how an extra capacitance emerges from the thermal fluctuations of the charges, which have been frozen in the Born-Oppenheimer ensemble of configurations where only the charge distribution $\mathbf{q}^*$ satisfying the constant-potential and electroneutrality constraints is considered explicitly.

Interestingly, given Eq. 31, an alternative derivation starting from the Born-Oppenheimer partition function Eq. 23 and considering $C_{\text{diff}} = \partial \langle Q_L^* \rangle^{\text{BO}}_{\mathbf{r}^N} / \partial\Delta\psi$, the additional term in the differential capacitance appears as $\langle \partial Q_L^* / \partial\Delta\psi \rangle^{\text{BO}}_{\mathbf{r}^N}$. Indeed, using Eq. 11 and $\frac{\partial \mathbf{q}^*}{\partial \Delta\psi} = \mathbf{S}\mathbf{D}$, we obtain the equality:

$$\left\langle \frac{\partial Q_L^*}{\partial \Delta\psi} \right\rangle^{\text{BO}}_{\mathbf{r}^N} = \left\langle \mathbf{D}^T \frac{\partial \mathbf{q}^*(\mathbf{r}^N)}{\partial \Delta\psi} \right\rangle^{\text{BO}}_{\mathbf{r}^N} = \left\langle \mathbf{D}^T\mathbf{S}\mathbf{D} \right\rangle^{\text{BO}}_{\mathbf{r}^N} = \mathbf{D}^T\mathbf{S}\mathbf{D} \,. \tag{38}$$

This allows us to interpret the extra capacitance $\mathbf{D}^T\mathbf{S}\mathbf{D}$ as the average response of the electrode to voltage for each microscopic configuration of the electrolyte, which was mentioned by Haskins and Lawson in Ref. 18. The present derivation further shows that it is independent of the microscopic configuration of the electrolyte as well as voltage, and provides an explicit expression from the $\mathbf{A}$ matrix describing the electrostatic interactions between all electrode atoms. This corresponds to the capacitance in the absence of any electrolyte,

$$C_{\text{diff}}^{\text{empty}} = \mathbf{D}^T\mathbf{S}\mathbf{D} \, . \tag{39}$$

It combines additively with the contribution arising from charge fluctuations induced by the thermal fluctuations of the electrolyte,

$$C_{\text{diff}}^{\text{electrolyte}} = \beta \left[\left\langle Q_L^{*2} \right\rangle_{\mathbf{r}^N}^{\text{BO}} - \left(\left\langle Q_L^{*} \right\rangle_{\mathbf{r}^N}^{\text{BO}} \right)^2 \right] = \beta \left\langle \delta Q_L^{*2} \right\rangle_{\mathbf{r}^N}^{\text{BO}} \, , \tag{40}$$

so that Eq. 37 corresponds to an equivalent circuit of capacitors in parallel.

A particularly simple expression in terms of the elements of the $\mathbf{A}^{-1}$ matrix can be obtained, if one introduces the following block decomposition:

$$\mathbf{A}^{-1} = \left(\begin{array}{c|c} (\mathbf{A}^{-1})_{LL} & (\mathbf{A}^{-1})_{LR} \\ \hline (\mathbf{A}^{-1})_{RL} & (\mathbf{A}^{-1})_{RR} \end{array} \right) \, , \tag{41}$$

with diagonal blocks of size $M_L \times M_L$ and $M_R \times M_R$ and off-diagonal blocks of size $M_L \times M_R$ and $M_R \times M_L$. Using simple matrix algebra, together with the definitions Eq. 21 of $\mathbf{S}$ and Eq. 7 of $\mathbf{D}$ and $\mathbf{E}$, one can show that the extra capacitance corresponding to the empty capacitor is given by

$$C_{\text{diff}}^{\text{empty}} = \mathbf{D}^T\mathbf{S}\mathbf{D} = \frac{\Sigma_{LL}\Sigma_{RR} - \Sigma_{LR}^2}{\Sigma_{LL} + \Sigma_{RR} + 2\Sigma_{LR}} \, , \tag{42}$$

where Σ_{LL}, Σ_{RR} and Σ_{LR} are the sums of the elements of the blocks defined in Eq. 41. In the particular but common case of identical electrodes, with $\alpha_L = -\alpha_R = 1/2$ and $\Sigma_{LL} = \Sigma_{RR}$, one also has the simple result $C_{\text{diff}} = \mathbf{D}^T\mathbf{A}^{-1}\mathbf{D} = (\Sigma_{LL} - \Sigma_{LR})/2$. In general, Eq. 42 provides a simple route to the calculation of the capacitance of arbitrarily shaped electrodes in a continuum dielectric, which could be used in the design of nano-structured capacitors[46].

III. APPLICATIONS

The analytical result Eq. 39 can be used to compute the differential capacitance of the empty capacitor, which also contributes to the differential capacitance in the presence of an electrolyte (see Eq. 37), if the matrix $\mathbf{A}$ can be inverted. In the limit of large systems, *i.e.* large number of electrode atoms and large distance between electrodes compared to their atomic structure, one should recover the result for an empty parallel plate capacitor with structureless electrodes, namely a capacitance per unit area $C_{\text{diff}}/\mathcal{A} = \varepsilon_0/L$, with ε_0 the vacuum permittivity and L the distance between the electrodes. Performing the matrix inversion explicitly becomes cumbersome when the number of atoms is large, so that it is difficult to take such a limit analytically. Nevertheless, we do recover it numerically, as shown below.

A. Systems and simulation details

In the present work, we consider several capacitors, illustrated in Figure 1: two empty capacitors, consisting of either graphite (panel a) or platinum (panel b) electrodes, and three graphite capacitors filled with pure water (panel c), a 1M NaCl aqueous electrolyte (panel d), or a room temperature ionic liquid, namely 1-butyl-3-methylimidazolium hexafluorophosphate (BMI-PF_6, panel e). We use the molecular dynamics code *MetalWalls* to run constant potential simulations with potential differences $\Delta\psi$ ranging from 0.0 to 20.0 V. Each electrode atom, regardless of the chemical species, has a Gaussian charge distribution of width $\eta^{-1} = 0.55$ Å. The charges $\mathbf{q}^*$ satisfying the constant-potential constraint are determined at each time step using a conjugate gradient minimization.

Two-dimensional boundary conditions are used with no periodicity in the z direction and we use an accurate 2D Ewald summation method to compute electrostatic interactions [22, 45]. We use a cutoff of 17 Å for both the short range part of the Coulomb interactions and the intermolecular interactions. For the latter we use the truncated and shifted Lennard-Jones potential. For graphite electrodes, the lateral box dimensions are 34.101×36.915 Å^2 with 5

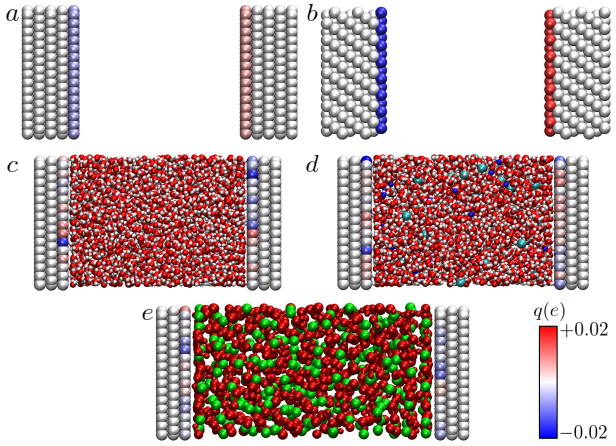


FIG. 1: Snapshots of the systems: (a) empty graphite capacitor (b) empty platinum capacitor (c) graphite capacitor with pure water (d) graphite capacitor with 1M NaCl aqueous electrolyte (e) graphite capacitor with BMI-PF_6 ionic liquid. The color scale indicates the charge of the electrode atoms for the considered configurations, at $\Delta\psi = 20$ V and 0 V for the empty and full capacitors, respectively.

atomic planes (*i.e.* 2400 carbon atoms) per electrode. For platinum, we consider the (111) surface of the *fcc* crystal structure with a lattice parameter $a = 3.9$ Å; the lateral box dimensions are 41.550×36.000 Å^2 with 8 atomic planes (*i.e.* 1800 platinum atoms) per electrode. For the filled capacitors, each graphite electrode has the same lateral dimensions as above with 3 atomic planes (*i.e.* 1440 carbon atoms) and the electrolytes are composed of 2160 SPC/E water molecules, 2160 SPC/E water molecules and 39 Na^+-Cl^- ion pairs, and 240 BMI^+-PF_6^- ion pairs, respectively. Force field parameters can be found in references 47–49 for water, 47–50 for aqueous NaCl and 49, 51 for BMI-PF_6. The volume of the simulation boxes is first equilibrated for 500 ps by performing simulations in which a constant force is applied to the electrodes, acting as rigid pistons, with magnitude corresponding to a force per unit area of 1 atm. It is then fixed for subsequent simulations by setting the electrodes separation to the equilibrium value: $L = 55.11$ Å, 56.2 Å, and 74.11 Å, respectively for water, aqueous NaCl and BMI-PF_6.

The equations of motion are integrated using the velocity-Verlet algorithm. Both water and the BMI^+ cation are treated as rigid molecules using the RATTLE algorithm[52]. Following the relevant experimental conditions, the aqueous systems are simulated at 298 K (with a timestep of 1 fs), whereas the ionic liquid is simulated at 400 K (with a larger timestep of 2 fs, allowed by the use of a coarse-grained model for the molecular ions), using a chain Nosé-Hoover thermostat. Charge values are sampled each 100 steps using trajectories of 4 ns for water, 6 ns for aqueous sodium chloride and 14 ns for BMI-PF_6 at a potential difference of $\Delta\psi = 0$ V. $C_{\text{diff}}^{\text{electrolyte}}$ is then computed from the variance of the total charge distribution and uncertainties correspond to the standard error on the variance, computed as: $\left\langle \delta Q_L^{*2} \right\rangle \times \sqrt{4\tau_C/\tau_S}$ where τ_S is the total sampling time and $\tau_C = \int_0^\infty \left\langle \delta Q_L^*(t)\delta Q_L^*(0) \right\rangle^2 / \left\langle \delta Q_L^{*2} \right\rangle^2 \mathrm{d}t$ is the correlation time.[53]

B. Electrolyte-free capacitors

The contribution of the empty capacitor can be computed from the positions of the electrode atoms and the width of the Gaussian charge distributions (which define the elements of the matrix $\mathbf{A}$) via Eq. 39. This result does not depend on voltage $\Delta\psi$, so that the charge of the empty capacitor should be proportional to $\Delta\psi$. Figure 2 compares this prediction for two empty capacitors, consisting of either graphite or platinum electrodes at different separations, with the charge determined numerically for several voltages. The numerical results confirm both the linear response, which means that the integral capacitance, $Q_L/\Delta\psi$ (ratio between the electrode charge and applied voltage), does not depend on voltage and is equal to the differential capacitance, C_{diff}, and that the slope is correctly predicted by Eq. 39 from the positions of the electrode atoms and the width of the Gaussian charge distributions. For large inter-electrode distances, the surface charge density is the same for both electrode types, whereas differences are observed for closer electrodes, due to their different atomic structures.

Figure 3 then shows the capacitance per unit area, $C_{\text{diff}}/\mathcal{A}$, as a function of the analytical result for structureless electrodes, ε_0/L, for the empty graphite capacitor, with distances L ranging between 10 and 200 Å. The numerical results for the atomically resolved electrodes converge to the analytical result for large inter-electrode distances, as

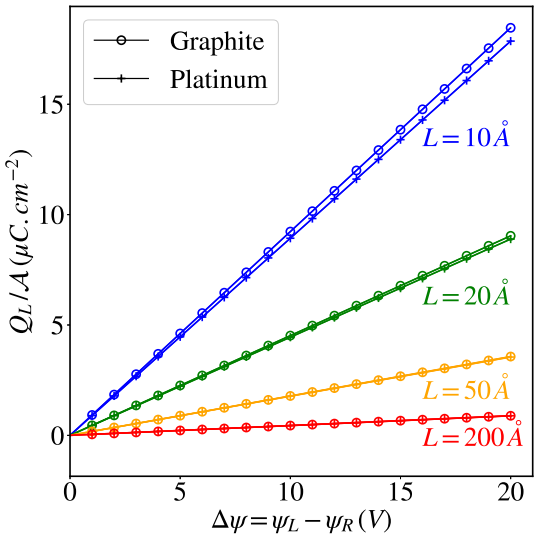


FIG. 2: Charge of the left electrode Q_L as a function of the applied voltage $\Delta\psi = \psi_L - \psi_R$, for the two empty graphite or platinum capacitors shown in Figs. 1a and b, respectively (see text for details). Results are shown for selected distances L between the first atomic planes of the electrodes, ranging from 10.0 to 200.0 Å. The symbols (∘ for graphite, + for platinum) indicate the charge determined numerically for various applied voltages between 1.0 and 20.0 V, while the lines are the predictions of Eq. 39.

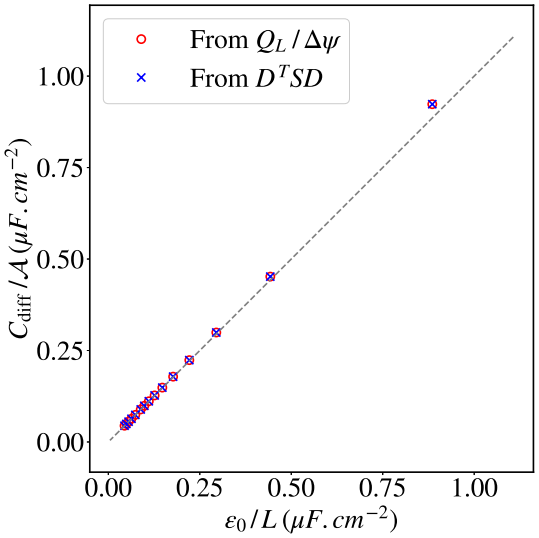


FIG. 3: Differential capacitance per unit area, $C_{\text{diff}}/\mathcal{A}$, with graphite electrodes as a function of the analytical prediction for an empty capacitor with structureless electrodes: ε_0/L, with $\mathcal{A}$ the area and L the distance between the electrodes ranging from 10 to 200 Å, for the empty capacitors (see Fig. 1a and b) at $\Delta\psi = 1.0V$. Red circles correspond to the slope of Fig. 2, while the blue crosses are the predictions from Eq. 39. The dashed line corresponds to $y = x$.

expected. Surprizingly, the difference is already small ($< 5\%$) for a distance $L = 10$ Å, which is not much larger than the distance between graphite planes (3.354 Å) or even the interatomic distance within planes (1.42 Å). The numerical results are in fact even better described as ε_0/L_{eff}, with an effective inter-electrode distance $L_{eff} = L - d$, with $d = 0.4$ Å comparable to the Gaussian width η^{-1} (not shown).

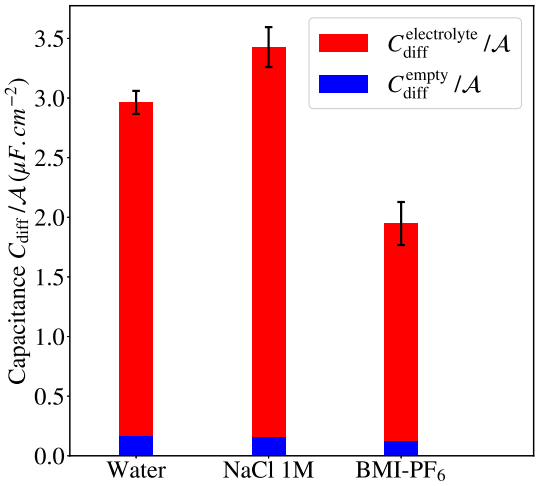


FIG. 4: Contributions to the differential capacitance per unit area $C_{\rm diff}/\mathcal{A}$ (see Eq. 37): from the empty capacitor, $C_{\rm diff}^{\rm empty} = \mathbf{D}^T\mathbf{S}\mathbf{D}$ and from the polarization fluctuations induced by the electrolyte, $C_{\rm diff}^{\rm electrolyte} = \beta\left\langle \delta Q_L^{*2}\right\rangle_{\mathbf{r}^N}^{\rm BO}$. Results are given for the three capacitors shown in panels c, d and e of Figure 1. Error bars correspond to standard errors for the variance corrected for data correlations (see text for computational details).

C. Full capacitors

We finally examine the relative contributions to the total differential capacitance in the presence of a liquid between the electrodes (see Eq. 37): that corresponding to the empty capacitor, $C_{\rm diff}^{\rm empty} = \mathbf{D}^T\mathbf{S}\mathbf{D}$, and that due to the thermal fluctuations of the electrolyte, $C_{\rm diff}^{\rm electrolyte} = \beta\left\langle \delta Q_L^{*2}\right\rangle_{\mathbf{r}^N}^{\rm BO}$. The results are shown on Figure 4 for the graphite capacitors containing either water, a 1M NaCl aqueous electrolyte or BMI-PF$_6$ (see panels c, d and e of Figure 1). In all cases, the contribution derived in this work, $C_{\rm diff}^{\rm empty}$, is small (between 5 and 6%) compared to $C_{\rm diff}^{\rm electrolyte}$ already obtained in Ref. 41 and comparable to the uncertainty on the latter. Such an observation is consistent with that of Haskins and Lawson [18] and explains why this additional contribution may have been forgotten in earlier work.

The value obtained for BMI-PF$_6$ is in good agreement to that reported for $C_{\rm diff}$ in Ref. 42, while that for 1M aqueous NaCl is comparable to the one obtained for the integral capacitance (average charge divided by voltage) at $\Delta\psi = 1\ V$ in Ref. 54. The increase in capacitance upon addition of salt to pure water, even though limited under the present conditions of concentration and inter-electrode distance, and the lower capacitance of ionic-liquid based capacitors compared to their solvent-based counterparts (acetonitrile in the case of BMI-PF$_6$), are also consistent with experimental trends and previously reported simulations [44, 55].

Additionally, for pure water, continuum dielectric theory predicts a total capacitance equal to $\varepsilon_0\varepsilon_r/L$, with ε_r the relative permittivity. Taking the value of $\varepsilon_r = 70.7$ for the SPC/E water model [56], this results in $C_{\rm diff} = 11.36\,\mu F.cm^{-2}$, which is $\sim 3-4$ times larger than the values obtained in the present work. This failure of the continuum picture is due to the fact that it does not capture the layering of water molecules close to the surface, due to their finite size and their orientation, due to hydrogen bonds, which result in a partial screening of the surface charge and in a decrease in the overall capacitance[24, 57, 58]. Far from the surfaces, however, the electric field is uniform and the corresponding dielectric constant decreases with increasing applied voltage[24, 58].

IV. CONCLUSIONS

We revisited the statistical mechanics of the constant-potential ensemble, for the generic case where the energy is a quadratic form of the fluctuating charges, by introducing explicitly the constraint of global electroneutrality of the system. We obtained explicit analytical results for a number of properties, including the configuration-dependent potential shift previously introduced as a Lagrange multiplier to enforce the electroneutrality constraint, as well as the configuration-dependent set of charges satisfying the constant-potential and electroneutrality constraints. We investigated the sampling of phase space corresponding to the full constant-potential ensemble and that achieved in the Born-Oppenheimer approximation, and discussed the possibility to compute observables with the latter. In particular, we showed that for any linear combination of atomic charges, in particular the total charge of the electrodes,

the average value is correctly sampled, while the fluctuations need to be corrected by a term for which we obtained an explicit expression. These results justify the use of Born-Oppenheimer dynamics to sample the constant-potential ensemble.

We derived an analytical expression for the differential capacitance of the system including an additional self-capacitance, as identified in Ref. 18, which we showed to be independent of voltage and of the configuration of the electrolyte. This term, which corresponds to the capacitance of the electrolyte-free capacitor, is expressible from the elements of the inverse of the matrix defining the quadratic form of the fluctuating charges in the energy. We illustrated numerically the validity of our results, and recovered in particular, at large inter-electrode distance, the expected result for an empty capacitor with structureless electrodes ($\varepsilon_0 \mathcal{A}/L$). By considering a variety of liquids between graphite electrodes, we confirmed that this contribution to the total differential capacitance is small compared to that induced by the thermal fluctuations of the electrolyte.

The present work applies to all classical electrode models with a Hamiltonian which can be expressed as a quadratic form of fluctuating charges. In particular, it is readily applicable to the semiclassical Thomas-Fermi model recently proposed to tune the metallicity of electrodes in molecular simulations [59], in order to interpret intriguing observations in Atomic Force Microscopy experiments on ionic liquids [60, 61]. It would be interesting to extend the present work to open systems, in which the exchange of electrolyte with a reservoir results in fluctuations in the number of ions and solvent molecules, which play an important role in the context of blue energy harvesting [62]. Other directions include the simulation of reactive systems [63] for electrochemical applications, as well as the coupling of electrical and mechanical properties, including forces induced by charge fluctuations [64] or to analyze recent Surface Force Balance experiments [65].

Conflicts of interest

There are no conflicts to declare.

Acknowledgements

It is a great pleasure to dedicate this article to Michiel Sprik, whose work has been an inspiration on many topics, including the classical molecular simulation of electrochemical systems, on the occasion of his 67^{th} birthday and retirement. BR and DTL were supported by the France-Berkeley Fund from the University of California, Berkeley. BR acknowledges financial support from the French Agence Nationale de la Recherche (ANR) under Grant No. ANR-17-CE09-0046-02 (NEPTUNE). This project has received funding from the European Research Council (ERC) under the European Union's Horizon 2020 research and innovation programme (grant agreement No. 771294).

[1] Y. Shao, J. Wang, H. Wu, J. Liu, I. A. Aksay and Y. Lin, *Electroanalysis*, 2010, **22**, 1027–1036.
[2] J. B. Goodenough and Y. Kim, *Chemistry of Materials*, 2010, **22**, 587–603.
[3] M. Salanne, B. Rotenberg, K. Naoi, K. Kaneko, P.-L. Taberna, C. P. Grey, B. Dunn and P. Simon, *Nat. Energy*, 2016, **1**, 16070.
[4] T. Bak, J. Nowotny, M. Rekas and C. C. Sorrell, *International Journal of Hydrogen Energy*, 2002, **27**, 991–1022.
[5] D. Brogioli, *Phys. Rev. Lett.*, 2009, **103**, 058501.
[6] R. Parsons, *Chem. Rev.*, 1990, **90**, 813–826.
[7] M. V. Fedorov and A. A. Kornyshev, *Chem. Rev.*, 2014, **114**, 2978–3036.
[8] J. Carrasco, A. Hodgson and A. Michaelides, *Nat. Mater.*, 2012, **11**, 667–674.
[9] A. Striolo, A. Michaelides and L. Joly, *Annu. Rev. Chem. Biomol. Eng.*, 2016, **7**, 533–556.
[10] C. Merlet, B. Rotenberg, P. A. Madden, P.-L. Taberna, P. Simon, Y. Gogotsi and M. Salanne, *Nature Mater.*, 2012, **11**, 306–310.
[11] C. Merlet, C. Péan, B. Rotenberg, P. A. Madden, B. Daffos, P.-L. Taberna, P. Simon and M. Salanne, *Nat. Commun.*, 2013, **4**, 2701.
[12] J. Vatamanu, O. Borodin, M. Olguin, G. Yushin and D. Bedrov, *J. Mater. Chem. A*, 2017, **5**, 21049–21076.
[13] O. Borodin, X. Ren, J. Vatamanu, A. von Wald Cresce, J. Knap and K. Xu, *Acc. Chem. Res.*, 2017, **50**, 2886–2894.
[14] M. Simoncelli, N. Ganfoud, A. Sene, M. Haefele, B. Daffos, P.-L. Taberna, M. Salanne, P. Simon and B. Rotenberg, *Phys. Rev. X*, 2018, **8**, 021024.
[15] C. Merlet, C. Péan, B. Rotenberg, P. Madden, P. Simon and M. Salanne, *J. Phys. Chem. Lett.*, 2013, **4**, 264–268.
[16] C. Merlet, B. Rotenberg, P. A. Madden and M. Salanne, *Phys. Chem. Chem. Phys.*, 2013, **15**, 15781–15792.
[17] K. Breitsprecher, K. Szuttor and C. Holm, *J. Phys. Chem. C*, 2015, **119**, 22445–22451.

[18] J. B. Haskins and J. W. Lawson, *J. Chem. Phys.*, 2016, **144**, 134701.
[19] J. Vatamanu, D. Bedrov and O. Borodin, *Mol. Simulat.*, 2017, **43**, 838.
[20] M. Girotto, A. P. dos Santos and Y. Levin, *J. Chem. Phys.*, 2017, **147**, 074109.
[21] J. I. Siepmann and M. Sprik, *J. Chem. Phys.*, 1995, **102**, 511–524.
[22] S. K. Reed, O. J. Lanning and P. A. Madden, *J. Chem. Phys.*, 2007, **126**, 084704.
[23] S. K. Reed, P. A. Madden and A. Papadopoulos, *J. Chem. Phys.*, 2008, **128**, 124701.
[24] A. P. Willard, S. K. Reed, P. A. Madden and D. Chandler, *Faraday Discuss.*, 2009, **141**, 423–441.
[25] A. P. Willard, D. T. Limmer, P. A. Madden and D. Chandler, *J. Chem. Phys.*, 2013, **138**, 184702.
[26] D. T. Limmer, A. P. Willard, P. Madden and D. Chandler, *Proc. Nat. Acad. Sci. USA*, 2013, **110**, 4200–4205.
[27] R. Burt, K. Breitsprecher, B. Daffos, P.-L. Taberna, P. Simon, G. Birkett, X. S. Zhao, C. Holm and M. Salanne, *J. Phys. Chem. Lett.*, 2016, **7**, 4015–4021.
[28] J. Vatamanu, O. Borodin and G. D. Smith, *J. Phys. Chem. B*, 2011, **115**, 3073–3084.
[29] Z. Li, G. Jeanmairet, T. Mendez-Morales, B. Rotenberg and M. Salanne, *The Journal of Physical Chemistry C*, 2018, **122**, 23917–23924.
[30] L. Pastewka, T. T. Järvi, L. Mayrhofer and M. Moseler, *Phys. Rev. B*, 2011, **83**, 165418.
[31] N. Onofrio and A. Strachan, *J. Chem. Phys.*, 2015, **143**, 054109.
[32] J. Johnson, *Phys. Rev.*, 1928, **32**, 97–109.
[33] H. Nyquist, *Phys. Rev.*, 1928, **32**, 110–113.
[34] U. Bertocci and F. Huet, *Corrosion*, 1995, **51**, 131–144.
[35] R. A. Cottis, *Corrosion*, 2001, **57**, 265–285.
[36] M. A. G. Zevenbergen, P. S. Singh, E. D. Goluch, B. L. Wolfrum and S. G. Lemay, *Anal. Chem.*, 2009, **81**, 8203–8212.
[37] P. S. Singh, H.-S. M. Chan, S. Kang and S. G. Lemay, *J. Am. Chem. Soc.*, 2011, **133**, 18289–18295.
[38] M. A. G. Zevenbergen, P. S. Singh, E. D. Goluch, B. L. Wolfrum and S. G. Lemay, *Nano Letters*, 2011, **11**, 2881–2886.
[39] N. Bonnet, T. Morishita, O. Sugino and M. Otani, *Phys. Rev. Lett.*, 2012, **109**, 266101.
[40] K. Kiyohara and K. Asaka, *J. Phys. Chem.*, 2007, **111**, 15903–15909.
[41] D. T. Limmer, C. Merlet, M. Salanne, D. Chandler, P. A. Madden, R. van Roij and B. Rotenberg, *Phys. Rev. Lett.*, 2013, **111**, 106102.
[42] C. Merlet, D. T. Limmer, M. Salanne, R. van Roij, P. A. Madden, D. Chandler and B. Rotenberg, *J. Phys. Chem. C*, 2014, **118**, 18291–18298.
[43] B. Rotenberg and M. Salanne, *J. Phys. Chem. Lett.*, 2015, **6**, 4978–4985.
[44] B. Uralcan, I. A. Aksay, P. G. Debenedetti and D. T. Limmer, *J. Phys. Chem. Lett.*, 2016, **7**, 2333.
[45] T. R. Gingrich and M. Wilson, *Chem. Phys. Letters*, 2010, **500**, 178–183.
[46] G. Yu, X. Xie, L. Pan, Z. Bao and Y. Cui, *Nano Energy*, 2013, **2**, 213–234.
[47] H. J. C. Berendsen, J. R. Grigera and T. P. Straatsma, *J. Phys. Chem.*, 1987, **91**, 6269–6271.
[48] T. Werder, J. H. Walther, R. L. Jaffe, T. Halicioglu and P. Koumoutsakos, *J. Phys. Chem. B*, 2003, **107**, 1345–1352.
[49] M. W. Cole and J. R. Klein, *Surf. Sci.*, 1983, **124**, 547–554.
[50] L. X. Dang, *J. Am. Chem. Soc.*, 1995, **117**, 6954–6960.
[51] D. Roy and M. Maroncelli, *J. Phys. Chem. B*, 2010, **114**, 12629–12631.
[52] H. C. Andersen, *Journal of Computational Physics*, 1983, **52**, 24–34.
[53] R. Zwanzig and N. K. Ailawadi, *Physical Review*, 1969, **182**, 280–283.
[54] N. Ganfoud, A. Sene, M. Haefele, A. Marin-Laflèche, B. Daffos, P.-L. Taberna, M. Salanne, P. Simon and B. Rotenberg, *Energy Storage Materials*, 2019, **21**, 190–195.
[55] C. Merlet, M. Salanne, B. Rotenberg and P. A. Madden, *Electrochimica Acta*, 2013, **101**, 262–271.
[56] M. Rami Reddy and M. Berkowitz, *Chemical Physics Letters*, 1989, **155**, 173–176.
[57] D. J. Bonthuis, S. Gekle and R. R. Netz, *Langmuir*, 2012, **28**, 7679–7694.
[58] G. Jeanmairet, B. Rotenberg, D. Borgis and M. Salanne, *J. Chem. Phys.*, 2019, **151**, 124111.
[59] T. Dufils, L. Scalfi, B. Rotenberg and M. Salanne, *Arxiv*, 2019, 1910.13341.
[60] J. Comtet, A. Niguès, V. Kaiser, B. Coasne, L. Bocquet and A. Siria, *Nat. Mater.*, 2017, **16**, 634–639.
[61] V. Kaiser, J. Comtet, A. Niguès, A. Siria, B. Coasne and L. Bocquet, *Faraday Discuss.*, 2017, **199**, 129–158.
[62] R. van Roij, *Electrostatics of Soft and Disordered Matter*, Pan Stanford Publishing, 2014, p. 263.
[63] K. A. Dwelle and A. P. Willard, *J. Phys. Chem. C*, 2019, **123**, 24095–24103.
[64] D. Drosdoff, I. V. Bondarev, A. Widom, R. Podgornik and L. M. Woods, *Phys. Rev. X*, 2016, **6**, 011004.
[65] C. S. Perez-Martinez and S. Perkin, *Soft Matter*, 2019, **15**, 4255–4265.